Article

Not peer-reviewed version

Increasing the Photovoltaic Efficiency of Semiconductor (Cu1-xAgx)2ZnSnS4 Thin Thin Films through Ag Content Modification

A. M. Bakry , Lamiaa El-Sherif , S. Hassaballa , Essam Shaaban *

Posted Date: 17 June 2024

doi: 10.20944/preprints202406.1053.v1

Keywords: CdS layer; (Cu1-xAgx)2ZnSnS4 thin layers; Structural analysis; Spectroscopic ellipsometry; Optical properties; Heterojunctions

Article

Increasing the Photovoltaic Efficiency of Semiconductor $(Cu_{1-x}Ag_x)_2ZnSnS_4$ Thin Thin Films Through Ag Content Modification

A. M. Bakry [1], L. S. El-Sherif [2,3], S. Hassaballa [4] and E. R. Shaaban [4,5,*]

[1] Department of Physics, College of Arts and Science in Wadi Al-Dawaser, Prince Sattam bin Abdulaziz University, Wadi Al-Dawaser 11991, Saudi Arabia, awad_bakry@yahoo.com
[2] Department of Physics, College of Arts and Science in Wadi Al-Dawaser, Prince Sattam bin Addulaziz University, Wadi-Dawaser 11991, Saudi Arabia. lamiaa_ph@yahoo.com
[3] Department of Physics, Faculty of Science, Ain Shams University, Cairo 11566, Egypt
[4] Physics Department, Faculty of Science, Islamic University of Madinah, Almadinah Al-Munawarah 42351, Saudi Arabia, Safwat_hassaballa@iu.edu.sa
[5] Department of Physics, Faculty of Science, Al-Azhar University, Assiut 71542, Egypt
* Correspondence: esam_ramadan2008@yahoo.com; Tel.: +201093344297

Abstract: The research that we are referring to examines the morphological, structural, and optical characteristics of kesterite (Cu1-xAgx)2ZnSnS4 (CAZTS) thin films, which are produced using a process known as thermal evaporation (TE). The study's main goal was to determine how different Ag contents affect the characteristics of CAZTS systems. X-ray diffraction (XRD) and Raman Spectroscopy: were used to confirm the crystal structure of the CAZTS thin films. Using a mathematical model of spectroscopic ellipsometry, the refractive index (n) represented the part of the complex refractive index, the extinction coefficient (k) portrayed the imaginary one, and also the energy band gap of the fabricated films were all calculated. The energy band gap of the thin films was also calculated. This is a crucial parameter for solar cell applications, as it determines the wavelength of light that the material can absorb. The energy band gap was found to decrease from 1.74 eV to 1.55 eV with increasing Ag content. The ITO/n-CdS/p-CAZTS/Mo heterojunction was well constructed, and the primary photovoltaic characteristics of the n-CdS/p-CAZTS junctions were examined for use in solar cells. Different Ag contents of the CAZTS layers were used to determine the dark and illumination (current-voltage) characteristics of the heterojunctions. The study's findings collectively point to CAZTS thin layers as potential absorber materials for solar cell applications.

Keywords: CdS layer; $(Cu_{1-x}Ag_x)_2ZnSnS_4$ thin layers; Structural analysis; Spectroscopic ellipsometry; Optical properties; Heterojunctions

1. Introduction

The growth of renewable energy sources, such as solar energy, is essential for lowering our reliance on fossil fuels and reducing the effects of climate change, to sum up. While there are still many obstacles to overcome in the development of PV technology, scientists working in the fields of materials science and nanotechnology are making great strides in the direction of solar cells that are highly efficient, inexpensive, and made of abundant natural materials [1]. Since many years ago, manufactured photovoltaic (PV) samples made of copper indium gallium selenide (CIGS) and cadmium telluride (CdTe) have been employed for commercial applications. They are renowned for having conversion efficiencies that are quite high in comparison to those of other thin-film PV technologies, which can reach up to 20% for CdTe and 22% for CIGS. These materials do, however, have a number of serious disadvantages that prevent their broad usage in the solar industry. The toxicity of these materials is one of the main problems. Cost is a further problem with CdTe and CIGS. Even though they are less expensive to create than conventional silicon-based PV systems, they are still rather expensive. Thin-film PV cells must be produced using complicated manufacturing

 doi:10.20944/preprints202406.1053.v1

procedures, which raises the cost of raw materials. Notwithstanding these disadvantages, standard silicon-based PV technologies have a number of benefits over CdTe and CIGS. They are appropriate for applications where weight and flexibility are key considerations, like building-integrated PV systems because they are lightweight and flexible. Additionally, they perform better in low-light circumstances and have a faster energy payback period, which means they can produce more energy overall than was needed to manufacture them. There has been an increase in interest recently in creating less harmful and pricey thin-film PV alternatives. Perovskite-based PV technologies are one approach that has shown promise in lab tests and is moving quickly toward industrialization. In comparison to CdTe and CIGS, perovskite-based PV cells have the potential to be more cost-effective, more efficient, less poisonous, and simpler to make. However, further study is required before they can be widely commercialized in order to overcome stability and durability difficulties [2,3].

In recent years, Cu_2ZnSnS_4 (CZTS), a quaternary material, has drawn a lot of interest as a promising absorber material for solar cell systems. It has a kesterite crystal structure and is composed of earth-abundant, non-toxic elements like zinc (Zn), tin (Sn), copper (Cu), and sulfur (S). Due to these characteristics, CZTS is a viable substitute for existing thin-film PV materials that use pricy and poisonous metals like cadmium (Cd) and indium (In). All things considered, CZTS is a promising material for thin-film PV applications because it is made up of numerous, non-toxic elements and has the right optical and electrical properties for solar cell technology. CZTS-based solar cells could replace conventional silicon-based and thin-film PV technologies as a result of additional study and development [4–7].

Since the spin coating is quick and inexpensive, it is a common technique for depositing CZTS thin films. The procedure entails coating a substrate with a thin layer of a precursor solution before rapidly spinning the substrate to equally disperse the solution. The precursor is then heated to form a solid CZTS coating on the substrate [8]. Another popular method for depositing CZTS thin films is sputtering. High-energy ions are used to bombard a target material in this process, causing atoms to be expelled and deposited onto a substrate. The composition and qualities of the CZTS film can be controlled by sputtering with a variety of gases, such as argon [9–11]. In thermal evaporation, the precursor substance is heated in a vacuum chamber until it vaporizes, and then allowed to deposit onto a substrate where it condenses into a solid film. High-quality CZTS films with good crystallinity and purity can be produced using this technique [12,13]. Pulsed Laser Deposition (PLD) is a process that ablates a target material with a high-energy laser before depositing it onto a substrate. With perfect control over the deposition rate and composition, this technique may make CZTS films that are very uniform, dense, and of the highest quality [14,15]. In order to generate a CZTS film, a preliminary film of electron-beam-evaporated precursors is heated in the presence of sulfur gas after being deposited onto a substrate by electron beam evaporation. Using this technique, superior CAZTS films with good regularity and crystallinity may be created [16,17]. In spray pyrolysis, a precursor solution is sprayed onto a hot substrate, which causes it to break down and produce a CZTS film. Although this technique is rather straightforward and can make large-area CZTS films, it can be difficult to regulate the film's thickness and homogeneity [18,19].

The PCE for pure CZTS solar cells is currently recorded at 9.2%, whereas the PCE for pure CZTSe solar cells is reported at 11.6%. Mixed CZTS/CZTSe solar cells have a PCE that is marginally higher at 12.6%. These efficiencies, however higher than those of CIGS and CdTe solar cells, which have shown efficiencies of up to 21.7%, are still below those of those solar cells. Notwithstanding their lower efficiency, CZTS-based solar cells continue to spark a lot of research interest because of their inexpensive, non-toxic, and readily available constituent materials. Researchers are investigating a number of methods to increase the stability and efficiency of CZTS-based solar cells, including optimizing deposition techniques, engineering the band structure, and creating new device topologies [20–23].

Highly effective $(Cu_{1-x}Ag_x)_2ZnSn(S,Se)_4$ solar cells were studied by Xue Yu and colleagues for the use in flexible Mo foil [23]. $Cu_2ZnSn(S,Se)_4$ encoded as (CZTSSe) junction' efficiency is significantly increased by cation substitution. The band gap of (CAZTSSe) thin layers can be changed in this study by doping with Ag_x (where x is the content of Ag ranging from 0 to 0.5. Additionally, it was

 doi:10.20944/preprints202406.1053.v1

discovered that Ag doping could clearly raise the CAZTSSe absorber's average grain size from 0.4 to 1.1 mm. Furthermore, the open-circuit voltage (Voc) steadily drops as a result. An increase in power conversion efficiency (PCE) from 4.34% to 6.24% was achieved.

The current investigation utilized thermal evaporation to create (Cu1-xAgx)2ZnSnS4 (CAZTS) thin films on pre-cleaned glasses to examine their structural and optical characteristics at various Ag concentrations (x ranging from 0 to 0.5). The study aimed to investigate the effects of Ag content on the structural, morphological, optical, and electrical characteristics of these extremely thin CAZTS layers. Additionally, spectroscopic ellipsometry was used for the first time to estimate the optical properties, including the energy gap, of the CAZTS films. Furthermore, the study assembled an ITO/n-CdS/p-CAZTS/Mo heterojunction, and the current density (J) – voltage (V) characteristics of these manufactured heterojunctions were analyzed for various CAZTS layers.

2. Experimental Techniques

2.1. Chemicals

Silver nitrate $Ag(NO_3)$ as a source for Ag, copper (II) nitrate $Cu(NO_3)_2$ for obtained Cu, zinc acetate $Zn(CH_3COO)_2$ for formating the Zn atoms, stannous chloride encoded as ($SnCl_2$), citric acid incarnated ($C_6H_8O_7$) form, deionized water, sulfide amine solution, and pure alcohol were the components used to synthesis the CAZTS thin layers. Without any additional purification, all of the used compounds and precursors were used.

2.2. Constructing CAZTS Layers

The silver, copper, zinc and antimony precursors mentioned in the chemicals section were used to prepare an aqueous solution prepared for the synthesis of CAZTS thin samples by dissolving mixtures of the four precursors in equal proportions equivalent to one mole/ liter. In order to produce a translucent solution, after 10 minutes of mixing and good stirring of the aqueous solution in the preparation flask, metal ions from the aforementioned precursors were added to citric acid ($C_6H_8O_7$) and deionized water. As a complexing agent, citric acid ($C_6H_8O_7$) was used. At 150°C, 6 mL of Sulphide amine solution was added to the flask and allowed to react for roughly 30 minutes. Following that, the CAZTS nanoparticles were separated via a centrifuge. Powder nanoparticles were dried in a vacuum oven to generate the CAZTS powder, which is the final product used to prepare thin films by thermal evaporation. These glass substrates were likewise cleaned with ultrasonic and allowed to air dry after numerous 30-minute rinses in distilled water and pure alcohol.

The vacuum unit or the DV 502 A-type coating device was set and calibrated at a deposition rate close to 20 angstrom/second and at high pressure in the vacuum chamber of 10^{-7} mbar, to obtain virgin thin films by the thermal evaporation method. The influence of film thickness was minimized by putting the same weight on the boat with the same thickness of thin films using the FTM6 thickness monitor. With astonishing accuracy, the film thickness was determined using a spectroscopic ellipsometry method.

2.3. Characterization and Measurements

The XRD patterns with Cu-$K_{\alpha 1}$ radiation (λ= 1.54056) measured by (Philips diffractometry (1710) device) were done to know the structure phase and the structural parameters such as the crystallite size and strain. **Raman Spectroscopy** technique was likely employed to further confirm the crystal structure and identify any structural defects or impurities. For studying surface morphology, a scanning electron microscope (SEM) with a 30 kV operating voltage is used. The spectroscopic ellipsometry (SE) method was used to investigate the optical characteristics. Using a SE technique with (VASE, J. A. Woollam Co., Inc.), data were collected via spectroscopic ellipsometry. Two parameters (ψ_{exp} and Δ_{exp}) were measured as a function of wavelength. The obtained data were gathered in the range from 300 to 1100 nm with an incidence angle of ~70°. The J. A. Woollam Complete Ease software program was used to analyze the SE data. The optical transmission and reflection spectra for th thin films were investigated using a double-beam computer-controlled

 doi:10.20944/preprints202406.1053.v1

spectrophotometer (UV-2101, Shimadzu) at a spectral range of wavelength from 300 to 2500 nm. The CdS thin layer was deposited directly on the CAZTS layer (200 nm) at different Ag content, which was deposited over the pre-cleaned glass substrates to fabricate the ITO (100 nm)/n-CdS/p-CAZTS /Mo(100 nm) heterojunctions. On the other hand, the Keithley 2400 device was used to measure the illumination (current-voltage, (I-V)) features with (AM1.5G) and (P_{in}=1800 mW/cm^2) produced by a 150W lamp under standard conditions for experimentation.

3. Results and Discussion

3.1. EDX and Structural Studies

A summary of the EDAX results of $(Cu_{1-x}Ag_x)_2ZnSnS_4$ thin layers is recorded in Table 1. The X-ray diffraction (XRD) patterns of $(Cu_{1-x}Ag_x)_2ZnSnS_4$ thin film with varying Ag content are presented in Figure 1(a). The XRD results confirm the formation of crystalline CAZTS phases. The CAZTS thin layers exhibit diffraction peaks at 28.53°, 47.32°, and 56.19°, corresponding to the diffraction planes of (112), (220), and (312), respectively. These planes are extracted from JCPDS card with no.26-0575. This provides strong evidence for the formation of CAZTS in a tetragonal phase. Furthermore, the CAZTS layers exhibit a sharper peak at (112) plane, indicating an improvement in crystal quality with an increase in Ag content. Figure 1 (b) illustrates the peak shift of (112) plane. A shift is observed in the diffraction angle towards smaller angles with increasing Ag content. The shift towards smaller diffraction angles in XRD (X-ray diffraction) curves with increasing Ag (silver) content can be attributed to a decrease in the interatomic distance between the atoms in the crystal lattice of the sample. The position of the diffraction peaks depends on the spacing between the atoms in the crystal lattice, which is determined by the atomic radii and the crystal structure. As the Ag atoms are substituted for other atoms in the crystal lattice, the interatomic distance between the atoms changes, leading to a shift in the position of the diffraction peaks. As Ag has a smaller atomic radius compared to the Cu element, the substitution of Ag atoms for Cu atoms results in a decrease in the interatomic distance, and thus a shift towards smaller diffraction angles in the XRD curve. This behavior can be used to identify the presence of Ag in a sample and to study the impacts of Ag substitution on the crystal structure and properties of the material [24–26].

The Debye-Scherrer equation is commonly used to determine the average crystallite size in polycrystalline materials from X-ray diffraction data. The equations relates the crystallite size (D) and lattice strain (e) to the main X-ray wavelength (λ), the diffraction angle (Bragg's angle θ), and the full width at half maximum (β) of the diffraction peak [26,27]:

$$D = \left(\frac{0.94}{\beta}\right).\frac{\lambda}{\cos\theta} \quad \& \quad e = \frac{\beta}{4\tan\theta} \quad \text{and} \quad \beta = \sqrt{\beta_{obs}^2 - \beta_{std}^2} \tag{1}$$

β is the widening equivalent of the difference in profile width between the films (β_{obs}) and the standard silicon (β_{std}).

Preprints.org (www.preprints.org) | NOT PEER-REVIEWED | Posted: 17 June 2024 doi:10.20944/preprints202406.1053.v1

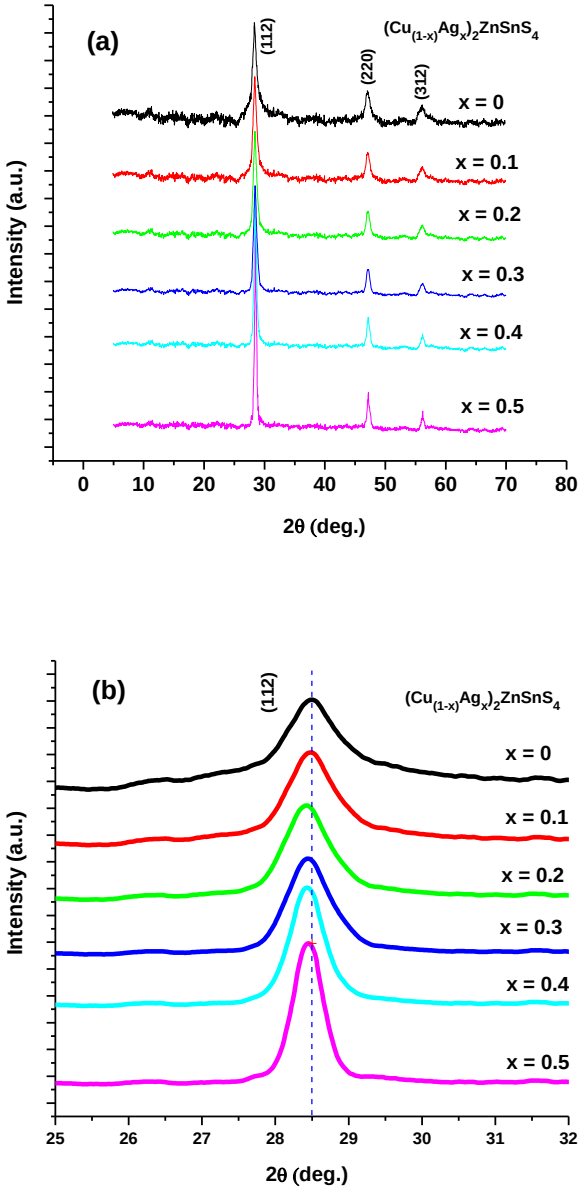

Figure 1. (a) XRD patterns of $(Cu_{(1-x)}Ag_x)_2ZnSnS_4$ thin films, (b) peak shift of (112) plane. .

Table 1. Summary of the EDAX results of (Cu1−xAgx)2ZnSnS4 thin films with various Ag contents (0, 0.1, 0.2, 0.3, 0.4, 0.5).

x	Cu (mV)	Ag (at/%)	Zn (at/%)	Sn (at/%)	S (at/%)
0	21.06	0	11.71	11.83	55.4
0.1	19.11	2.03	11.81	11.94	55.11
0.2	17.21	4.05	11.78	11.93	55.03
0.3	15.04	6.12	11.68	11.91	55.25
0.4	12.88	8.52	11.82	11.87	54.91
0.5	10.88	10.21	11.85	11.93	55.13

The size of the crystallites increased as a result of increasing the Ag content, as seen in Figure 2, whereas the lattice strain values dropped with increasing Ag concentration. The size of crystallites

 doi:10.20944/preprints202406.1053.v1

rises when Ag content increases because it serves as a site of nucleation for the development of new crystals or as a catalyst for the production of existing crystals. This is due to the possibility of extra nucleation sites for crystal growth being provided by the existence of Ag atoms, which encourages the building of bigger crystals. Lattice strain, on the other hand, measures the departure from the ideal crystal structure and can be caused by a variety of things, such as impurities or flaws in the crystal lattice. Because more Ag atoms can aid in reducing strain in the crystal lattice, the lattice strain values decrease as the Ag content rises. This is since Ag atoms have a higher atomic radius than the host metal atoms, which can cause the crystal lattice to be distorted. More Ag atoms are integrated into the lattice as the Ag concentration rises, which can aid in restoring the optimum crystal structure and lowering lattice strain. Overall, as a result of Ag's influences on crystal development and lattice distortion, an increase in Ag concentration causes crystallites to grow larger and lattice strain values to drop.

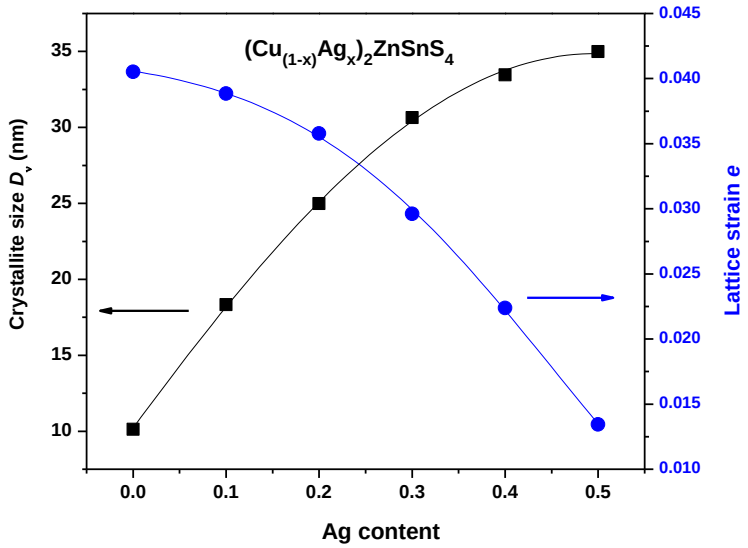

Figure 2. Crystallite size and lattice strain of $(Cu_{(1-x)}Ag_x)_2ZnSnS_4$ thin films as a function of Ag content.

3.2. Morphological Properties

With a focus on the impact of increasing Ag concentration, (SEM) were utilized to notice the surface morphological state of the CAZTS thin layers. The surface characteristics of the samples under study are depicted in the SEM images in Figure 3 and the particle size diagram is illustrated in Figure 4. According to SEM images, the first CAZTS film had a rough, uneven surface and obvious voids in its structural frame. The CAZTS film's surface structure, however, was significantly impacted by the addition of Ag content. The films became more homogeneous and compact with tightly packed grains that had specific structural characteristics. As a consequence, the rest films had fewer voids and appeared smoother than the first. The grain and its limits could be seen more clearly in the SEM images as the Ag content rose. Overall, the SEM images showed that increasing Ag concentration significantly enhanced the surface morphology of the CAZTS thin films, leading to more uniform, tightly packed, and identifiable grain patterns. This may result in a smoother, more predictable surface morphology and a more equal distribution of atoms on the surface. As a result, the grain patterns are more clearly defined and closely packed. Additionally, the crystal structure of the CAZTS thin films can be changed by the addition of Ag. As a result, more homogeneous and smaller grains may form, further enhancing the thin films' surface morphology. This phenomenon can be linked to the fact that Ag's crystal structure differs from CAZTS's, which can alter how the thin films'

 doi:10.20944/preprints202406.1053.v1

crystals arise. SEM images have generally demonstrated that raising the Ag content in CAZTS thin films can greatly improve their surface morphology, resulting in more regular, densely packed, and recognizable grain patterns. This enhancement can be attributed to Ag's capacity to change the crystal structure of the thin films in addition to its surfactant effect on the formation of the thin films.

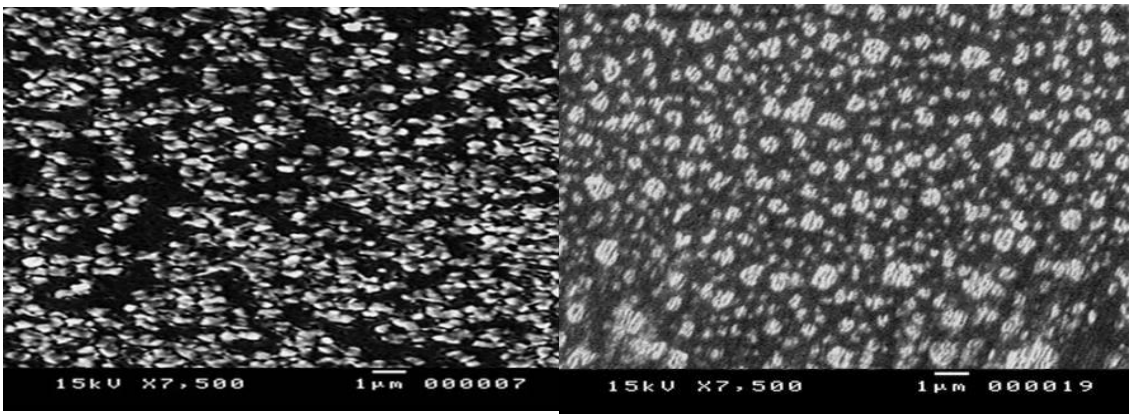

x=0 x=0.2

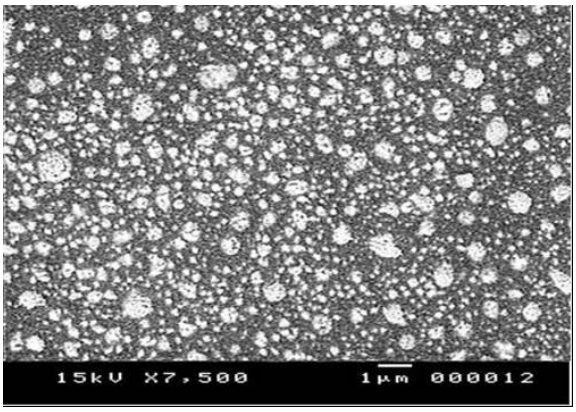

x=0.5

Figure 3. SEM images of $(Cu_{(1-x)}Ag_x)_2ZnSnS_4$ thin films (a) x = 0, (b) x = 0.2 and (c) x = 0.5.

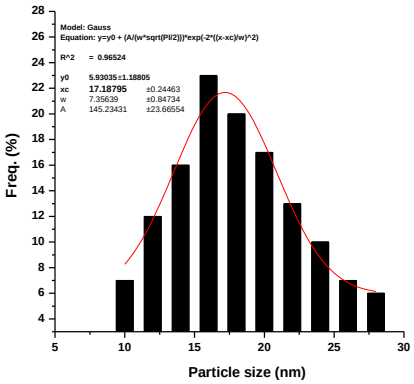

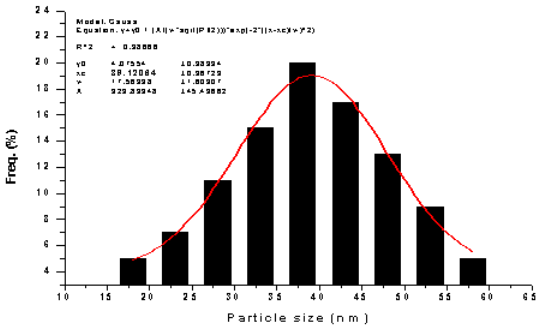

Preprints.org (www.preprints.org) | NOT PEER-REVIEWED | Posted: 17 June 2024 doi:10.20944/preprints202406.1053.v1

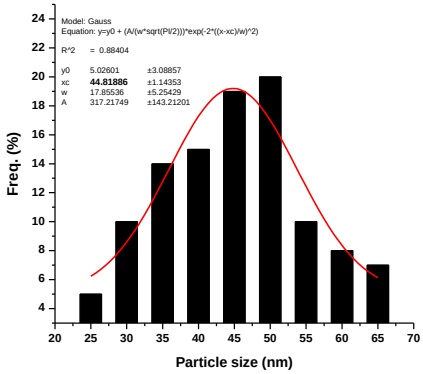

Figure 4. Particle size of $(Cu_{(1-x)}Ag_x)_2ZnSnS_4$ thin films (a) x = 0, (b) x = 0.2 and (c) x = 0.5.

3.3. Raman Spectra

To determine the phase structure and crystallinity of the CAZTS thin films, Raman spectroscopy was used. The CAZTS samples' acquired Raman spectra, which in turn were captured in the spectral range between 100 and 600 cm^{-1}, were discovered to be remarkably similar. The three unique Raman modes in the spectra, with strong peaks at 286 cm^{-1} and 340 cm^{-1}, corresponded to the Kesterite structure of CAZTS. These results imply that the CAZTS thin films were naturally crystalline and extremely pure. Consequently, the Raman analysis offered additional evidence in favor of the development of CAZTS thin films with desired properties [25–27]. Figure 5 displays a graphic depiction of the Raman spectra. The primary peak seen at 340 cm^{-1} in the Raman spectra transitions to lower energies as the Ag content rises. The presence of internal stress in the CAZTS layers is responsible for this shift. This phenomenon has been previously reported in CAZTS layers [23,28]. According to the Raman spectroscopy data, weak peaks were observed at 476 cm^{-1}, which can be due to the presence of the Cu_2S phase.

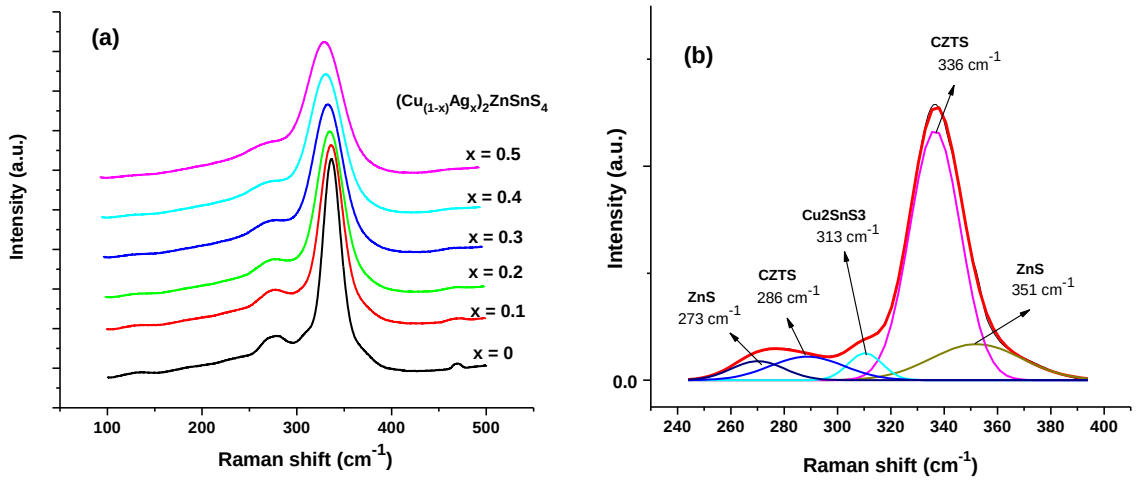

Figure 5. (a) Raman spectra of $(Cu_{(1-x)}Ag_x)_2ZnSnS_4$ thin films and (b) deconvolution of at x = 0.

3.4. Spectroscopic Ellipsometry

The optical constants (n, k) and thickness (d) of CAZTS thin films can have a considerable impact on their performance attributes, and spectroscopic ellipsometry (SE) is a widely used method to precisely characterize these features. SE is an important optical method that monitors polarisation shifts in light reflected from surfaces. By analyzing the changes in the polarization of light, SE can

 doi:10.20944/preprints202406.1053.v1

provide information on the optical constants of thin layers, including their refractive index, extinction coefficient, and thickness. SE can also be used to study the anisotropic properties of materials, such as birefringence. For CAZTS thin films, accurate knowledge of the optical constants is crucial for optimizing the performance of the films in photovoltaic and optoelectronic applications. The (n and k) constants of the films determine the absorption and reflection of light, which can have a significant impact on the efficiency of solar cells or other devices that rely on the absorption of light. By using SE to measure the reflectance and phase shift of light at multiple wavelengths and incident angles, it is possible to accurately determine the optical constants of CAZTS layers. These measurements can then be used to model the optical properties of the films and optimize their performance in specific applications. Additionally, SE can also be used to determine the thickness of the CAZTS layers, which is another critical parameter for device performance. Accurate acquaintance of the film thickness can be utilized to optimize the fabrication process and ensure consistent performance across multiple devices. In summary, SE is a powerful technique for accurately characterizing the optical properties of CAZTS films, which is crucial for optimizing their performance in photovoltaic and optoelectronic applications.

The formula connecting the spectroscopic ellipsometric parameters Ψ and Δ Fresnel's factor of the polarized light can be given as follows [29–31]:

$$\rho = \frac{r_p}{r_s} = tan\,\psi\, exp(i\Delta) \tag{2}$$

Here, r_p and r_s portray Fresenal's factor of the parallel polarized wave (p) and perpendicularly polarized wave (s). The ellipsometric (ψ_{exp} and Δ_{exp}) of CAZTS /glass layers among a outcome of studied CAZTS is illustrated in Figure 6. The measurements are frequently made in spectroscopic ellipsometry at various wavelengths (in this case, every 5 nm from 300 to 1100 nm), and the values of and are noted at each wavelength. Using 1'modeling software, these data can then be utilized to determine the complicated refractive index and thickness of the CAZTS film. The plane of incidence, which is the plane where light beams are incident and reflected, and the surface normal of the CAZTS film are at an angle of 70 degrees. In order to examine the anisotropic characteristics of thin films, this angle is frequently employed in spectroscopic ellipsometry.

A three-layer optical approach, with the substrate composed of glass as the first layer, the CAZTS absorber layer as the following one, and the surface roughness layer as the last layer, was used to calculate (n, k, and d) of the studied CAZTS layers. In addition, the Complete EASE software's Cauchy version of the belt was used to simulate the glass layers while the B-spline computational method was used to model the CAZTS layers. Effective medium approximation (EMA) is used to model rough layers, which is a useful tool for determining the morphology of multilayers [32–35].

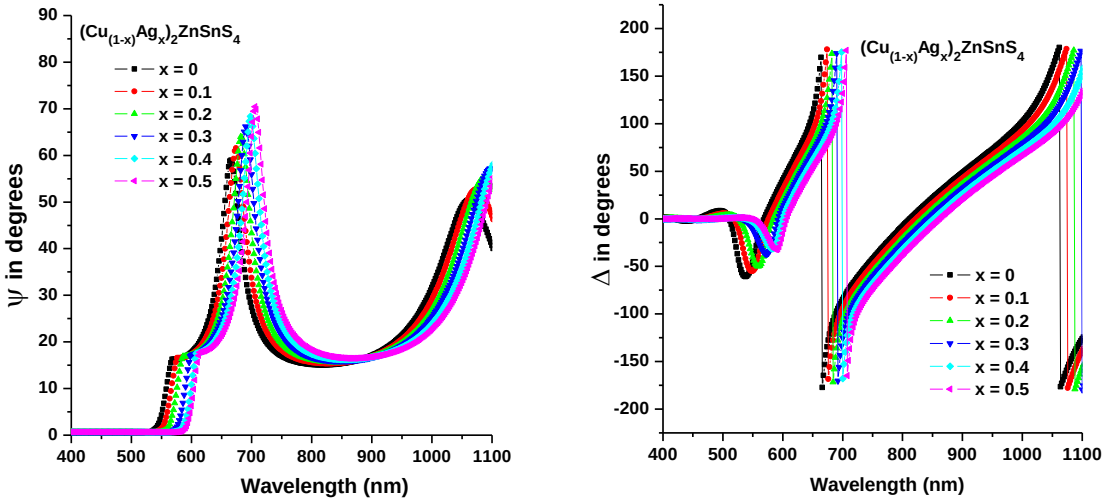

Preprints.org (www.preprints.org) | NOT PEER-REVIEWED | Posted: 17 June 2024 doi:10.20944/preprints202406.1053.v1

Figure 6. Spectral ellipsometric data ψ & Δ for $(Cu_{(1-x)}Ag_x)_2ZnSnS_4$ thin films grown on glass substrate.

Figure 7(a, b) illustrates the spectral various of $\psi_{exp.}$, Δ_{exp} for the last sample, which agree with the computed ψ_i^{cal}, Δ_i^{cal} data observed via the mentioned model. When these figures were fitted, the low Mean Square Error (MSE) values ranged from 2.46 to 2.35 as the studied thin films' Ag content grew from 0 to 0.5%Ag and the CAZTS layer's surface roughness increased from 3.70 nm to 2.75 nm. The coherence of the reflection pairs in the thin film is another factor that contributes to the interference arrangement in the spectrum of light [36]. The main fitted (n and k) constants of studied layers are illustrated in Figure 8 and Figure 9, respectively. Due to the increase in crystallinity caused by the larger crystallize size, the n-spectra grows as the Ag content increases in CAZTS layers [37,38]. Figure 8 shows the k-spectra of the CAZTS/glass layer obtained using the model averred above. Importantly lower k values are obviously detected at the absorption edge, verifying that the light is completely absorbed by the fabricated layers [39].

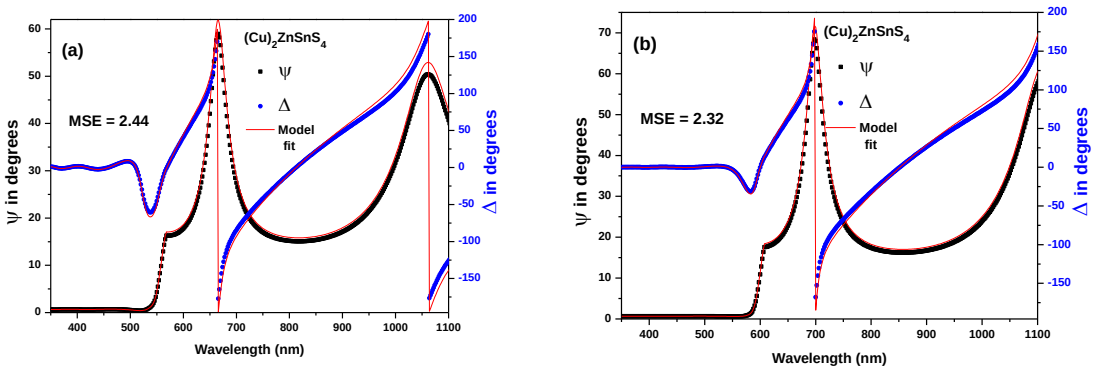

Figure 7. Spectral ellipsometric data ψ and Δ for $(Cu_{(1-x)}Ag_x)_2ZnSnS_4$ thin films for (a) x = 0 and (b) x = 0.4 grown on glass substrate. Experimental results are indicated by symbols, and the solid lines represent the model fit data.

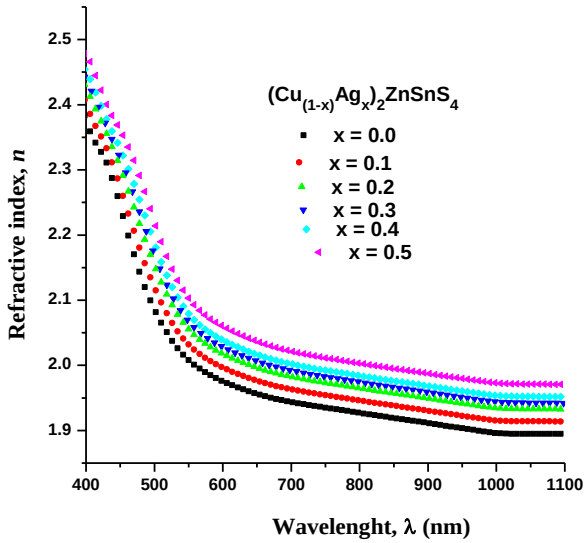

Figure 8. Dispersion refractive index for $(Cu_{(1-x)}Ag_x)_2ZnSnS_4$ thin films.

 doi:10.20944/preprints202406.1053.v1

The formula: $\alpha = 4\pi k/\lambda$ relates the absorption coefficient (α) to the absorption index (k) and wavelength (λ). The proportion of incident light absorbed by a substance per unit route length is indicated by the absorption index (k), a dimensionless quantity. The absorption coefficient (α), which is impacted by a different of variables including the composition, thickness, and microstructure of the material, offers information on how strongly the material absorbs light at a specific wavelength in the instance of CAZTS/glass layers with varied Ag contents. One may ascertain the optical characteristics of these materials and their prospective uses in optoelectronics, photovoltaics, and other sectors by determining the absorption coefficient for varied Ag concentrations of CAZTS/glass layers [40].

CAZTS materials are quaternary semiconductors that have undergone substantial research in preparation for their prospective application in photovoltaic solar cells. Efficiency as a solar absorber is greatly influenced by the material's optical properties, particularly its energy band gap. For extracting the energy band gap of semiconductors, researchers frequently utilize the Tauc expression. It is based on a material's ability to absorb photons of a particular energy, as determined by the material's absorption coefficient. The following can be used to express the Tauc expression [41–43]:

$$(\alpha h\nu) \quad = \alpha_o (h\nu - E_g)^P \tag{3}$$

In this formula, p and α_o incarnate exponent and constant. The index value, p is a parameter that depends on the nature of the band gap (direct or indirect) and determines the transition type from VB to CB. For the polycrystalline character of the CAZTS layers under investigation, the permitted direct transition is dominant with (p = 1/2) [44–46]. Figure 10 shows the plotting of $(\alpha h\nu)^2$ versus hν for different Ag contents of CAZTS layer. The energy band gap E_g^{opt} was determined by subtracting the measured data's intercept from the absorption coefficient's linear extrapolation to zero after the measured data had been fitted to the Tauc expression. As the Ag concentration in the CAZTS layers increases, the band gap value for the CAZTS/glass film drops (see Figure 11) as sigmoidal behavior. This is due to the possibility that the addition of Ag will cause some Zn and/or Cu sites in the CAZTS lattice to partially substitute. The band gap of the material decreases as a result, the impact of doping Ag (silver) atoms into a CAZTS (Copper Zinc Tin Sulfide) lattice, specifically how it affects the band gap of the material. Silver (Ag) has a lower electronegativity compared to Zinc (Zn) or Copper (Cu). Electronegativity is a measure of an element's tendency to attract electrons towards itself in a chemical bond. Because Ag has a lower electronegativity, it's more willing to give up its electrons. When Ag atoms are doped into the CAZTS lattice, they contribute electrons to the lattice. This is due to the lower electronegativity of Ag. These extra electrons can affect the electronic structure of the material. The extra electrons from the Ag doping contribute to the conduction band of the material. The conduction band is the energy band in a material where electrons are free to move and conduct electricity. When there are more electrons in the conduction band, the band gap decreases. Lowering the band gap means it requires less energy to excite an electron from the valence band (where electrons are normally located) to the conduction band [47–49],. This can have implications for the material's optical and electronic properties. Several other factors besides doping can affect the decrease of band gap of a material. These include structural factors[50], defects in the lattice and stress in the material's surface [51–53].

 doi:10.20944/preprints202406.1053.v1

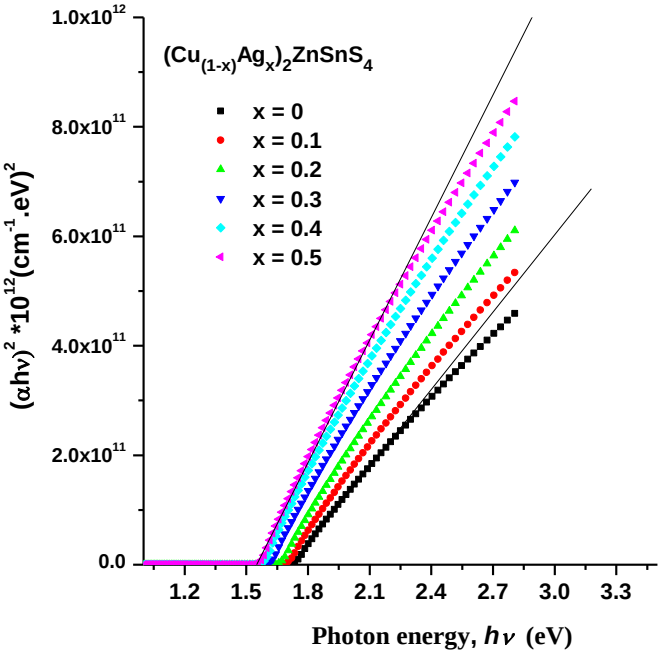

Figure 10. Variations of $(\alpha h\nu)^2$ versus photon energy ($h\nu$) for $(Cu_{(1-x)}Ag_x)_2ZnSnS_4$ thin films.

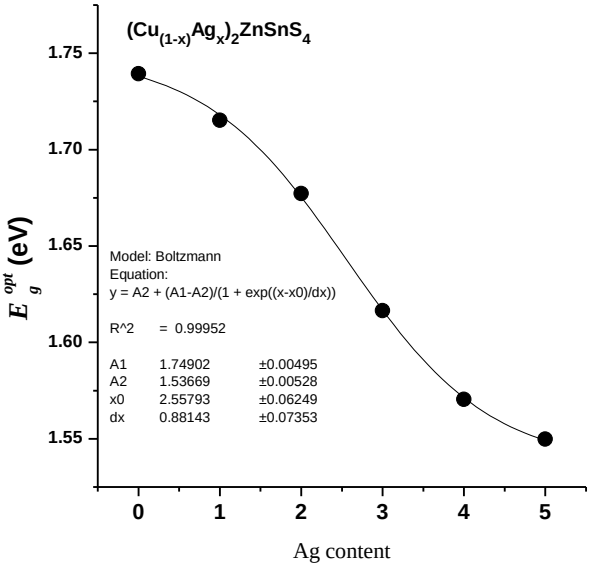

Figure 11. Optical energy gap of $(Cu_{(1-x)}Ag_x)_2ZnSnS_4$ thin films as a function of Ag content.

The transmission and reflection spectra of (Cu1−xAgx)2ZnSnS4 thin films with different Ag concentrations (0, 0.1, 0.2, 0.3, 0.4, 0.5) are displayed in Figure 12. The transmittance in transparent regions increases as the Ag content rises, according to these figures, whereas the reflectance decreases as the Ag level rises. The improvement in transmittance with increasing Ag content for $Cu_{1-x}Ag_x)_2ZnSnS_4$ thin films could also be related to changes in the crystal structure or morphology of the thin films. Ag substitution could lead to a more orderly crystal structure or reduce defects that otherwise absorb or scatter light, thus enhancing transparency. Also, Higher Ag content might result

 doi:10.20944/preprints202406.1053.v1

in smoother film surfaces, reducing scattering losses and allowing for better transmission of light through the material. But, the decrease in reflectance with increasing Ag content suggests alterations in the surface and electronic structure that make the surface less reflective. This could be due to a smoother surface, as mentioned, or changes in the electronic states at the surface, affecting how light interacts with the material. Increased Ag content might be improving optical impedance matching between the film and its substrate, thus reducing the amount of light reflected from the surface. This effect would enhance the efficiency of optical devices by minimizing energy losses due to reflection. A decrease in reflectance, coupled with an increase in transmission in specific regions, might also suggest that absorption in other wavelength regions could be changing. This is critical for applications like photovoltaics, where controlling absorption profiles is essential for maximizing efficiency. The described changes in the optical properties of $(Cu1-xAgx)2ZnSnS4$ thin films with different Ag concentrations have significant implications for photovoltaic applications, particularly in designing more efficient solar cells. By tailoring the Ag content, it might be possible to optimize these materials for maximum light absorption and conversion efficiency, leveraging the enhanced transmission and reduced reflectance.

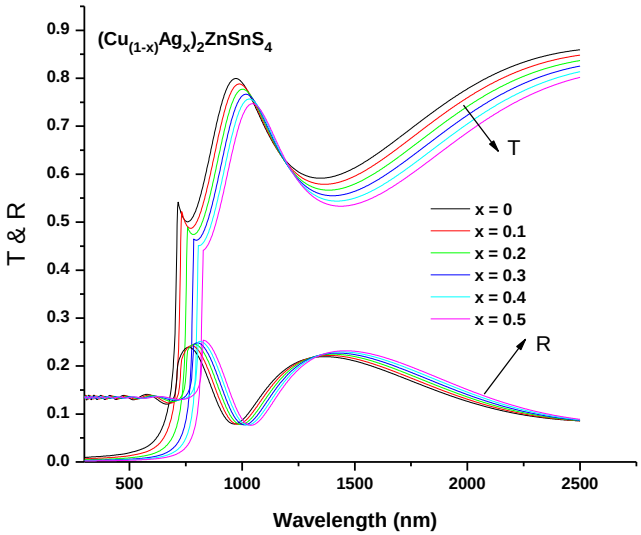

Figure 12. Transmission and Reflection spectra of $(Cu_{(1-x)}Ag_x)_2ZnSnS_4$ thin films.

3.5. Features of p-n Junction

The main diagram of the examined junction is shown in Figure 13. One should be aware that CAZTS extracts the key solar cell fabrication parameters to predict how the illumination (J-V) characteristics will behave. The applied voltage and the current are connected, and the formula described in the Ref. [53] provides the remaining properties of the manufactured diode. Figure 14(a) shows the illumination (J-V) characterization of junctions. Figure 14(b) shows the illumination (P-V) characterization of junctions under illumination in forward bias conditions. When a (P-V) cell is illuminated and operated in forward bias, it generates power due to the photovoltaic effect. The power conversion efficiency (PCE) of these devices is a critical parameter, indicating how efficiently they can convert sunlight into electrical energy. In the forward bias, the (P-V) characteristics in the illumination case are illustrated in Figure 14 (b). The $PCE = P_{\max} \times \left(P_{in}\right)^{-1} \%$ formula [54,55], (which $P_{\max}$ incarnates the maximum power in Figure 13 (b), and P_{in} is the experimental value of input power) helped us in the calculation of the power conversion efficiency (PCE) for the generated devices. On the other side, the fill factor (FF) is computed utilizing $FF = \left((V_{\max} . I_{\max}) \times (V_{OC} . I_{SC})^{-1} \right) = P_{\max} \times (V_{OC} . I_{SC})^{-1}$ [54,55]. Here, V_{oc} is the open-circuit voltage,

 doi:10.20944/preprints202406.1053.v1

the voltage measured across the terminals of the PV cell when no current is flowing (i.e., when the circuit is open). I_{sc} is the short-circuit current, the current that flows when the cell's terminals are shorted together (i.e., when the voltage across the cell is zero). The V_{max} and I_{max} are the voltage and the current corresponding to the maximum power points P_{max} . The fill factor is a dimensionless number that ranges between 0 and 1, often expressed as a percentage. Higher fill factor values indicate a more square-like I-V characteristic curve, suggesting that the solar cell is capable of operating closer to its V_{oc} and I_{sc} under load, which in turn implies higher efficiency and quality of the solar cell. Figure 15 (a) shows the behavior of J_{sc} and V_{oc} and Figure 15 (b) also shows the behavior FF-η curves as a function of Ag content of $(Cu_{(1-x)}Ag_x)_2ZnSnS_4$ thin films. As shown in Figure 15 (b) the (PCE) in the illumination state with increasing Ag content which corresponds to x = 0.4 and 0.5 % Ag results confirms that the layer with the largest silver content is the best for use in the solar cells in this work. By substituting Ag for Cu in the kesterite structure, the essentially tuning the electrical properties of the material. Silver has a higher electrical conductivity and incorporating it into the lattice can enhance the charge carrier mobility within the semiconductor. Higher mobility reduces the resistive losses within the cell, allowing for more efficient charge transport from the point of generation to the collection electrodes.The introduction of Ag, known for its strong plasmonic resonances, can significantly impact the optical properties of the solar cell. These resonances can lead to improved light trapping within the semiconductor layer, as metallic nanoparticles or inclusions scatter and absorb light, increasing the path length of photons in the material. This results in more light absorption and, consequently, a higher generation rate of electron-hole pairs, which is critical for enhancing the cell's photocurrent and overall efficiency. The doping or substitution process involving Ag can also influence the crystalline structure of the $(Cu_{(1-x)}Ag_x)_2ZnSnS_4$ thin films. By potentially forming a more ordered crystalline lattice or healing defects that would otherwise act as recombination centers, Ag incorporation can enhance the quality of the semiconductor. Fewer recombination sites mean that once generated, charge carriers (electrons and holes) have a higher probability of reaching the electrodes before recombining, effectively increasing the carrier lifetime and the device's efficiency. The combined effects of increased charge carrier mobility, enhanced light trapping due to plasmonic effects, and improved material quality leading to reduced recombination all contribute to the overall increase in the solar cell's efficiency.

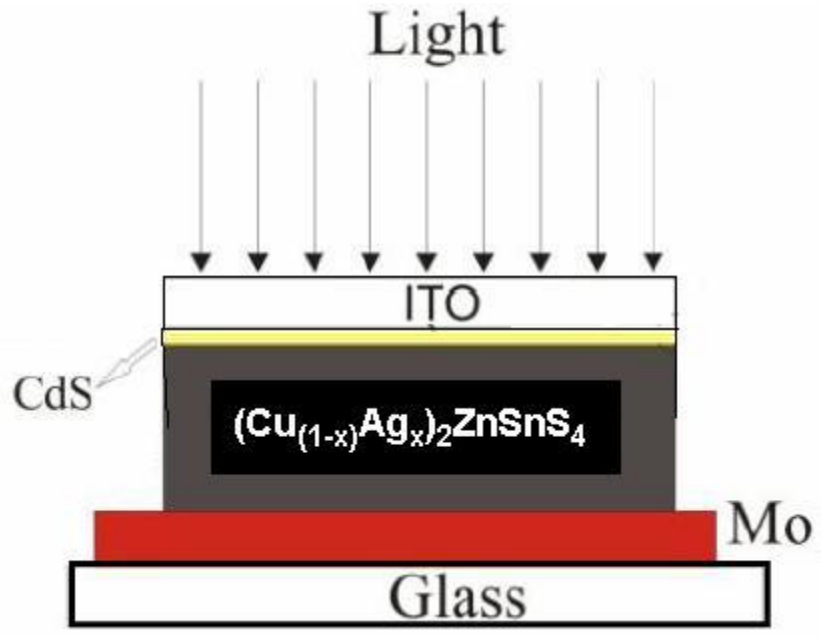

Figure 13. the basic structure of $(Cu_{(1-x)}Ag_x)_2ZnSnS_4$ solar cell.

Preprints.org (www.preprints.org) | NOT PEER-REVIEWED | Posted: 17 June 2024 doi:10.20944/preprints202406.1053.v1

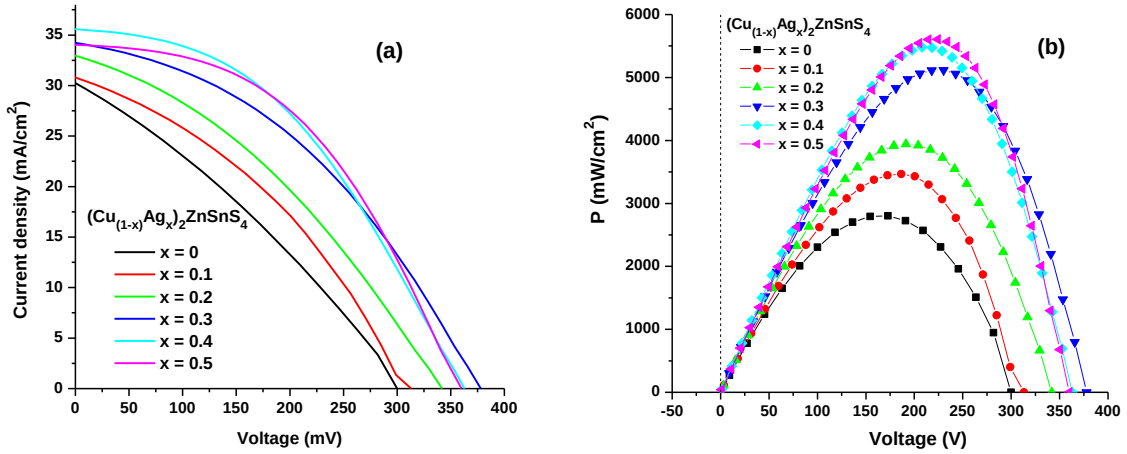

Figure 14. (a) J-V and (b) P-V curves of of $(Cu_{(1-x)}Ag_x)_2ZnSnS_4$ thin films.

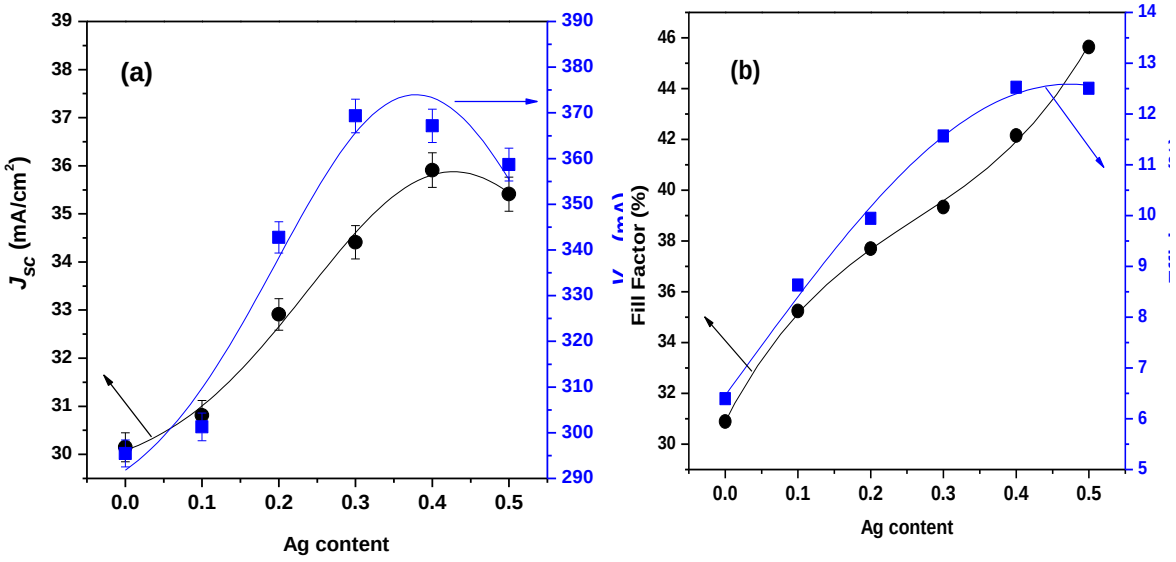

Figure 15. (a) Jsc-Voc and (b) FF-η curves of of $(Cu_{(1-x)}Ag_x)_2ZnSnS_4$ thin films.

4. Conclusions

This work investigated the effects of varying the Ag content on the structural, morphological, and optical properties of thin layers of CAZTS, which were prepared via the thermal evaporation method. The XRD patterns revealed that the thin layers had a Kesterite band structure, with a crystallite size ranging from 11 to 33 nm. The optical properties of the CAZTS/glass film were found to improve with increasing Ag content, as demonstrated by an increase in the optical constants n and k. Additionally, the direct transition energy decreased from 1.74 to 1.55 eV. Since Ag atoms increase electrons to the CAZTS lattice when they are doped, the results also established that the produced heterojunctions' optical properties improved with increasing Ag content. Ag has a lower electronegativity, which clarifies this. The material's electrical structure may be impacted by these additional electrons. The material's conduction band is improved by the additional electrons from the Ag doping. When a photovoltaic cell is worked in forward bias with illumination, it products power. One important factor that displays how well these devices can change sunlight into electrical energy is their power conversion efficiency (PCE). A more square-like I-V characteristic curve, indicated by greater fill factor values, proposes that the solar cell can operate closer to its Voc and Isc under load, indicating higher efficiency and quality of the solar cell. The layer with the highest silver

 doi:10.20944/preprints202406.1053.v1

concentration is the best for use in the solar cells in this work, as confirmed by the (PCE) in the illumination state with increasing Ag content, which corresponds to x = 0.4 and 0.5 Ag results. All things considered, this work offers insightful information on the characteristics and behavior of CAZTS thin layers with different Ag contents, information that may help advance the formation of solar cell technologies that are more effective.

Acknowledgments: This study is supported via funding from Prince sattam bin Abdulaziz University project number (PSAU/2023/R/1445).

References

1. Mitzi, David B., Min Yuan, Wei Liu, Andrew J. Kellock, S. Jay Chey, Vaughn Deline, and Alex G. Schrott. "A high-efficiency solution-deposited thin-film photovoltaic device." *Advanced Materials* 20, no. 19 (2008): 3657-3662. https://doi.org/10.1002/adma.200800555.
2. Nguyen, Thi Hiep, Takato Kawaguchi, Jakapan Chantana, Takashi Minemoto, Takashi Harada, Shuji Nakanishi, and Shigeru Ikeda. "Structural and Solar Cell Properties of a Ag-Containing Cu2ZnSnS4 Thin Film Derived from Spray Pyrolysis." *ACS applied materials & interfaces* 10, no. 6 (2018): 5455-5463. https://doi.org/10.1021/acsami.7b14929.
3. Bär, M., I. Repins, M. A. Contreras, L. Weinhardt, R. Noufi, and C. Heske. "Chemical and electronic surface structure of 20%-efficient Cu (In, Ga) Se 2 thin film solar cell absorbers." *Applied Physics Letters* 95, no. 5 (2009): 05210. https://doi.org/10.1063/1.3194153.
4. Sun, Rujun, Daming Zhuang, Ming Zhao, Qianming Gong, Mike Scarpulla, Yaowei Wei, Guoan Ren, and Yixuan Wu. "Beyond 11% efficient Cu2ZnSn (Se, S) 4 thin film solar cells by cadmium alloying." *Solar Energy Materials and Solar Cells* 174 (2018): 494-498. https://doi.org/10.1016/j.solmat.2017.09.043.
5. Todorov, Teodor K., Kathleen B. Reuter, and David B. Mitzi. "High-efficiency solar cell with earth-abundant liquid-processed absorber." *Advanced materials* 22, no. 20 (2010): E156-E159. https://doi.org/10.1002/adma.200904155.
6. Fernandes, P. A., Salomé, P. M. P., & Da Cunha, A. F., CuxSnSx+ 1 (x= 2, 3) thin films grown by sulfurization of metallic precursors deposited by dc magnetron sputtering. physica status solidi c, 7 (2010) 901-904. https://doi.org/10.1002/pssc.200982746.
7. Sun, R., et al., *Beyond 11% efficient Cu 2 ZnSn (Se, S) 4 thin film solar cells by cadmium alloying.* Solar Energy Materials and Solar Cells, 2018. 174: p. 494-498. https://doi.org/10.1016/j.solmat.2017.09.043.
8. Lee, Seul Gi, Jongmin Kim, Huyn Suk Woo, Yongcheol Jo, A. I. Inamdar, S. M. Pawar, Hyung Sang Kim, Woong Jung, and Hyun Sik Im. "Structural, morphological, compositional, and optical properties of single step electrodeposited Cu2ZnSnS4 (CZTS) thin films for solar cell application." *Current Applied Physics* 14, no. 3 (2014): 254-258. https://doi.org/10.1016/j.cap.2013.11.028.
9. Lincot, Daniel, Jean-François Guillemoles, S. Taunier, D. Guimard, J. Sicx-Kurdi, A. Chaumont, O. Roussel et al. "Chalcopyrite thin film solar cells by electrodeposition." *Solar Energy* 77, no. 6 (2004): 725-737. https://doi.org/10.1016/j.solener.2004.05.024.
10. Cunningham, D., M. Rubcich, and D. Skinner. "Cadmium telluride PV module manufacturing at BP Solar." *Progress in Photovoltaics: Research and Applications* 10, no. 2 (2002): 159-168. https://doi.org/10.1002/pip.417.
11. Ahmed, Shafaat, Kathleen B. Reuter, Oki Gunawan, Lian Guo, Lubomyr T. Romankiw, and Hariklia Deligianni. "A high efficiency electrodeposited Cu2ZnSnS4 solar cell." *Advanced Energy Materials* 2, no. 2 (2012): 253-259. https://doi.org/10.1002/aenm.201100526.
12. Farinella, Marta, Rosalinda Inguanta, Tiziana Spanò, P. Livreri, S. Piazza, and C. Sunseri. "Electrochemical deposition of CZTS thin films on flexible substrate." *Energy Procedia* 44 (2014): 105-110. https://doi.org/10.1016/j.egypro.2013.12.015.
13. Ge, Jie, and Yanfa Yan. "Controllable multinary alloy electrodeposition for thin-film solar cell fabrication: a case study of kesterite Cu2ZnSnS4." *iScience* 1 (2018): 55-71. https://doi.org/10.1016/j.isci.2018.02.002.
14. Schäfer, W., and Rudolf Nitsche. "Tetrahedral quaternary chalcogenides of the type Cu2 II IV S4 (Se4)." *Materials Research Bulletin* 9, no. 5 (1974): 645-654. https://doi.org/10.1016/0025-5408(74)90135-4.
15. Wang, K., O. Gunawan, T. Todorov, B. Shin, S. J. Chey, N. A. Bojarczuk, D. Mitzi, and S. Guha. "Thermally evaporated Cu 2 ZnSnS 4 solar cells." *Applied Physics Letters* 97, no. 14 (2010): 143508. https://doi.org/10.1063/1.3499284.
16. Shin, Byungha, Oki Gunawan, Yu Zhu, Nestor A. Bojarczuk, S. Jay Chey, and Supratik Guha. "Thin film solar cell with 8.4% power conversion efficiency using an earth-abundant Cu2ZnSnS4 absorber." *Progress in Photovoltaics: Research and Applications* 21, no. 1 (2013): 72-76. https://doi.org/10.1002/pip.1174.
17. Tiwari, Kunal J., Raju Chetty, Ramesh Chandra Mallik, and P. Malar. "Solid state synthesis and e-beam evaporation growth of Cu2ZnSnSe4 for solar energy absorber applications." *Solar Energy* 153 (2017): 173-180. https://doi.org/10.1016/j.solener.2017.05.042.

 doi:10.20944/preprints202406.1053.v1

18. Katagiri, Hironori, Kazuo Jimbo, Satoru Yamada, Tsuyoshi Kamimura, Win Shwe Maw, Tatsuo Fukano, Tadashi Ito, and Tomoyoshi Motohiro. "Enhanced conversion efficiencies of Cu2ZnSnS4-based thin film solar cells by using preferential etching technique." *Applied physics express* 1, no. 4 (2008): 041201. https://doi.org/10.1143/APEX.1.041201.
19. Jimbo, Kazuo, Ryoichi Kimura, Tsuyoshi Kamimura, Satoru Yamada, Win Shwe Maw, Hideaki Araki, Koichiro Oishi, and Hironori Katagiri. "Cu2ZnSnS4-type thin film solar cells using abundant materials." *Thin solid films* 515, no. 15 (2007): 5997-5999. https://doi.org/10.1016/j.tsf.2006.12.103.
20. Seboui, Zeineb, Yvan Cuminal, and Najoua Kamoun-Turki. "Physical properties of Cu2ZnSnS4 thin films deposited by spray pyrolysis technique." *Journal of Renewable and Sustainable Energy* 5, no. 2 (2013): 023113. https://doi.org/10.1063/1.4795399.
21. Hong, Chang Woo, Seung Wook Shin, Mahesh P. Suryawanshi, Myeng Gil Gang, Jaeyeong Heo, and Jin Hyeok Kim. "Chemically deposited CdS buffer/kesterite Cu2ZnSnS4 solar cells: relationship between CdS thickness and device performance." *ACS applied materials & interfaces* 9, no. 42 (2017): 36733-36744. https://doi.org/10.1021/acsami.7b09266.
22. Nguyen, Thi Hiep, Takato Kawaguchi, Jakapan Chantana, Takashi Minemoto, Takashi Harada, Shuji Nakanishi, and Shigeru Ikeda. "Structural and Solar Cell Properties of a Ag-Containing Cu2ZnSnS4 Thin Film Derived from Spray Pyrolysis." *ACS applied materials & interfaces* 10, no. 6 (2018): 5455-5463. https://doi.org/10.1021/acsami.7b14929.
23. Cazzaniga, Andrea, Andrea Crovetto, Chang Yan, Kaiwen Sun, Xiaojing Hao, Joan Ramis Estelrich, Stela Canulescu et al. "Ultra-thin Cu2ZnSnS4 solar cell by pulsed laser deposition." *Solar Energy Materials and Solar Cells* 166 (2017): 91-99. https://doi.org/10.1016/j.solmat.2017.03.002.
24. Moholkar, A. V., S. S. Shinde, A. R. Babar, Kyu-Ung Sim, Ye-bin Kwon, K. Y. Rajpure, P. S. Patil, C. H. Bhosale, and J. H. Kim. "Development of CZTS thin films solar cells by pulsed laser deposition: influence of pulse repetition rate." *Solar Energy* 85, no. 7 (2011): 1354-1363. https://doi.org/10.1016/j.solener.2011.03.017.
25. Lokhande, A. C., R. B. V. Chalapathy, J. S. Jang, P. T. Babar, M. G. Gang, C. D. Lokhande, and Jin Hyeok Kim. "Fabrication of pulsed laser deposited Ge doped CZTSSe thin film based solar cells: Influence of selenization treatment." *Solar Energy Materials and Solar Cells* 161 (2017): 355-367. https://doi.org/10.1016/j.solmat.2016.12.016.
26. Agawane, G. L., S. A. Vanalakar, A. S. Kamble, A. V. Moholkar, and J. H. Kim. "Fabrication of Cu2 (ZnxMg1-x) SnS4 thin films by pulsed laser deposition technique for solar cell applications." *Materials Science in Semiconductor Processing* 76 (2018): 50-54. https://doi.org/10.1016/j.mssp.2017.12.010.
27. Guo, Qijie, Grayson M. Ford, Wei-Chang Yang, Bryce C. Walker, Eric A. Stach, Hugh W. Hillhouse, and Rakesh Agrawal. "Fabrication of 7.2% efficient CZTSSe solar cells using CZTS nanocrystals." *Journal of the American Chemical Society* 132, no. 49 (2010): 17384-17386. https://doi.org/10.1021/ja108427b.
28. Kim, Jongmin, C. Park, S. M. Pawar, Akbar I. Inamdar, Yongcheol Jo, J. Han, JinPyo Hong et al. "Optimization of sputtered ZnS buffer for Cu2ZnSnS4 thin film solar cells." *Thin Solid Films* 566 (2014): 88-92. https://doi.org/10.1016/j.tsf.2014.07.024.
29. Barkhouse, D. Aaron R., Oki Gunawan, Tayfun Gokmen, Teodor K. Todorov, and David B. Mitzi. "Device characteristics of a 10.1% hydrazine-processed Cu2ZnSn (Se, S) 4 solar cell." *Progress in Photovoltaics: Research and Applications* 20, no. 1 (2012): 6-11. https://doi.org/10.1002/pip.1160.
30. Wang, Wei, Mark T. Winkler, Oki Gunawan, Tayfun Gokmen, Teodor K. Todorov, Yu Zhu, and David B. Mitzi. "Device characteristics of CZTSSe thin-film solar cells with 12.6% efficiency." *Advanced Energy Materials* 4, no. 7 (2014): 1301465. https://doi.org/10.1002/aenm.201301465.
31. Lee, Seul Gi, Jongmin Kim, Huyn Suk Woo, Yongcheol Jo, A. I. Inamdar, S. M. Pawar, Hyung Sang Kim, Woong Jung, and Hyun Sik Im. "Structural, morphological, compositional, and optical properties of single step electrodeposited Cu2ZnSnS4 (CZTS) thin films for solar cell application." *Current Applied Physics* 14, no. 3 (2014): 254-258. https://doi.org/10.1016/j.cap.2013.11.028.
32. Sun, R., et al., *Beyond 11% efficient Cu 2 ZnSn (Se, S) 4 thin film solar cells by cadmium alloying*. Solar Energy Materials and Solar Cells, 2018. 174: p. 494-498. https://doi.org/10.1016/j.solmat.2017.09.043.
33. Sun, Kaiwen, Fangyang Liu, Chang Yan, Fangzhou Zhou, Jialiang Huang, Yansong Shen, Rong Liu, and Xiaojing Hao. "Influence of sodium incorporation on kesterite Cu2ZnSnS4 solar cells fabricated on stainless steel substrates." *Solar Energy Materials and Solar Cells* 157 (2016): 565-571. https://doi.org/10.1016/j.solmat.2016.07.036.
34. Liu, Xu, Jialiang Huang, Fangzhou Zhou, Fangyang Liu, Kaiwen Sun, Chang Yan, John A. Stride, and Xiaojing Hao. "Understanding the key factors of enhancing phase and compositional controllability for 6% efficient pure-sulfide Cu2ZnSnS4 solar cells prepared from quaternary wurtzite nanocrystals." *Chemistry of Materials* 28, no. 11 (2016): 3649-3658. https://doi.org/10.1021/acs.chemmater.5b04620.
35. Ericson, Tove, Fredrik Larsson, Tobias Törndahl, Christopher Frisk, Jes Larsen, Volodymyr Kosyak, Carl Hägglund, Shuyi Li, and Charlotte Platzer-Björkman. "Zinc-Tin-Oxide Buffer Layer and Low Temperature

Post Annealing Resulting in a 9.0% Efficient Cd-Free Cu2ZnSnS4 Solar Cell." *Solar RRL* 1, no. 5 (2017): 1700001. https://doi.org/10.1002/solr.201700001.

36. Hong, Chang Woo, Seung Wook Shin, Mahesh P. Suryawanshi, Myeng Gil Gang, Jaeyeong Heo, and Jin Hyeok Kim. "Chemically deposited CdS buffer/kesterite Cu2ZnSnS4 solar cells: relationship between CdS thickness and device performance." *ACS applied materials & interfaces* 9, no. 42 (2017): 36733-36744. https://doi.org/10.1021/acsami.7b09266.
37. Erkan, Mehmet Eray, Vardaan Chawla, and Michael A. Scarpulla. "Reduced defect density at the CZTSSe/CdS interface by atomic layer deposition of Al2O3." *Journal of Applied Physics* 119, no. 19 (2016): 194504. https://doi.org/10.1063/1.4948947.
38. Crovetto, Andrea, Chang Yan, Beniamino Iandolo, Fangzhou Zhou, John Stride, Jørgen Schou, Xiaojing Hao, and Ole Hansen. "Lattice-matched Cu2ZnSnS4/CeO2 solar cell with open circuit voltage boost." *Applied Physics Letters* 109, no. 23 (2016): 233904. https://doi.org/10.1063/1.4971779.
39. Messaoud, Khaled Ben, Marie Buffière, Guy Brammertz, Nick Lenaers, Hans-Gerd Boyen, Sylvester Sahayaraj, Marc Meuris, Mosbah Amlouk, and Jef Poortmans. "Synthesis and characterization of (Cd, Zn) S buffer layer for Cu2ZnSnSe4 solar cells." *Journal of Physics D: Applied Physics* 50, no. 28 (2017): 285501. https://doi.org/10.1088/1361-6463/aa76b7.
40. Li, Jianjun, Xiaoru Liu, Wei Liu, Li Wu, Binghui Ge, Shuping Lin, Shoushuai Gao et al. "Restraining the Band Fluctuation of CBD-Zn (O, S) Layer: Modifying the Hetero-Junction Interface for High Performance Cu2ZnSnSe4 Solar Cells with Cd-Free Buffer Layer." *Solar Rrl* 1, no. 10 (2017): 1700075. https://doi.org/10.1002/solr.201700075.
41. Bras, Patrice, and Jan Sterner. "Influence of H2S annealing and buffer layer on CZTS solar cells sputtered from a quaternary compound target." In *2014 IEEE 40th Photovoltaic Specialist Conference (PVSC)*, pp. 0328-0331. IEEE, 2014. https://doi.org/10.1109/PVSC.2014.6924924.
42. Nagoya, A., R. Asahi, and G. Kresse. "First-principles study of Cu2ZnSnS4 and the related band offsets for photovoltaic applications." *Journal of Physics: Condensed Matter* 23, no. 40 (2011): 404203. https://doi.org/10.1088/0953-8984/23/40/404203.
43. Akram, Muhammad Aftab, Sofia Javed, Mohammad Islam, Mohammad Mujahid, and Amna Safdar. "Arrays of CZTS sensitized ZnO/ZnS and ZnO/ZnSe core/shell nanorods for liquid junction nanowire solar cells." *Solar Energy Materials and Solar Cells* 146 (2016): 121-128. https://doi.org/10.1016/j.solmat.2015.11.034.
44. Qasem, A., Hassan, A. A., Rajhi, F. Y., Abbas, H. A. S., & Shaaban, E. R. (2022). Effective role of cadmium doping in controlling the linear and non-linear optical properties of non-crystalline Cd–Se–S thin films. Journal of Materials Science: Materials in Electronics, 33(4), 1953-1965. https://doi.org/10.1007/s10854-021-07400-5.
45. Sun, Kaiwen, Chang Yan, Fangyang Liu, Jialiang Huang, Fangzhou Zhou, John A. Stride, Martin Green, and Xiaojing Hao. "Over 9% efficient kesterite Cu2ZnSnS4 solar cell fabricated by using Zn1−xCdxS buffer layer." *Advanced Energy Materials* 6, no. 12 (2016): 1600046. https://doi.org/10.1002/aenm.201600046.
46. Qasem, A., Alshahrani, B., Yakout, H. A., Abbas, H. A. S., & Shaaban, E. R. (2021). Tuning structural, optical, electrical and photovoltaic characteristics of n-type CdS1− xSbx layers for optimizing the performance of n-(CdS: Sb)/p-Si solar cells. Applied Physics A, 127(11), 1-13. https://doi.org/10.1007/s00339-021-04999-4
47. Yan, Chang, Fangyang Liu, Kaiwen Sun, Ning Song, John A. Stride, Fangzhou Zhou, Xiaojing Hao, and Martin Green. "Boosting the efficiency of pure sulfide CZTS solar cells using the In/Cd-based hybrid buffers." *Solar Energy Materials and Solar Cells* 144 (2016): 700-706. https://doi.org/10.1016/j.solmat.2015.10.019.
48. Platzer-Björkman, Charlotte, Christoper Frisk, J. K. Larsen, Tove Ericson, S-Y. Li, J. J. S. Scragg, Jan Keller, Fredrik Larsson, and Tobias Törndahl. "Reduced interface recombination in Cu2ZnSnS4 solar cells with atomic layer deposition Zn1− x Sn x O y buffer layers." *Applied Physics Letters* 107, no. 24 (2015): 243904. https://doi.org/10.1063/1.4937998.
49. Yang, Kee-Jeong, Jun-Hyoung Sim, Boram Jeon, Dae-Ho Son, Dae-Hwan Kim, Shi-Joon Sung, Dae-Kue Hwang et al. "Effects of Na and MoS2 on Cu2ZnSnS4 thin-film solar cell." *Progress in Photovoltaics: Research and Applications* 23, no. 7 (2015): 862-873. https://doi.org/10.1002/pip.2500.
50. Zhou, Fangzhou, Fangqin Zeng, Xu Liu, Fangyang Liu, Ning Song, Chang Yan, Aobo Pu, Jongsung Park, Kaiwen Sun, and Xiaojing Hao. "Improvement of J sc in a Cu2ZnSnS4 Solar Cell by Using a Thin Carbon Intermediate Layer at the Cu2ZnSnS4/Mo Interface." *ACS applied materials & interfaces* 7, no. 41 (2015): 22868-22873. https://doi.org/10.1021/acsami.5b05652.
51. Jia, Jinhuan, Yongfeng Li, Bin Yao, Zhanhui Ding, Rui Deng, Yuhong Jiang, and Yingrui Sui. "Band offsets of Ag2ZnSnSe4/CdS heterojunction: An experimental and first-principles study." *Journal of Applied Physics* 121, no. 21 (2017): 215305. https://doi.org/10.1063/1.4984315.
52. Qasem, A., Alrafai, H. A., Alshahrani, B., Said, N. M., Hassan, A. A., Yakout, H. A., & Shaaban, E. R, Adapting the structural, optical and thermoelectrical properties of thermally annealed silver selenide (AgSe) thin films for improving the photovoltaic characteristics of the fabricated n-AgSe/p-CdTe solar cells. Journal of Alloys and Compounds, 899 (2022) 163374. https://doi.org/10.1016/j.jallcom.2021.163374.

 doi:10.20944/preprints202406.1053.v1

53. Yeh, Min-Yen, Po-Hsun Lei, Shao-Hsein Lin, and Chyi-Da Yang. "Copper-zinc-tin-sulfur thin film using spin-coating technology." *Materials* 9, no. 7 (2016): 526. https://doi.org/10.3390/ma9070526.
54. Elsaeedy, H. I., Qasem, A., Yakout, H. A., & Mahmoud, M. "The pivotal role of TiO2 layer thickness in optimizing the performance of TiO_2/P-Si solar cell." Journal of Alloys and Compounds 867 (2021): 159150. https://doi.org/10.1016/j.jallcom.2021.159150.
55. Assem, E. E., Ashour A., Shaaban E. R., Qasem A. "Implications changing of the CdS window layer thickness on photovoltaic characteristics of n-CdS/i-AgSe/p-CdTe solar cells." Chalcogenide Letters 19.11 (2022). https://doi.org/ 10.15251/CL.2022.1911.825.